AFRL-AFOSR-UK-TR-2014-0034

Quantifying Space Environment Interactions with Debris Objects using Observation Data Fusion Techniques

Thomas Schildknecht
Monika Hager

UNIVERSITAET BERN
NON-PROFIT STATE UNIVERSITY
HOCHSCHULSTRASSE 4
BERN 3012 SWITZERLAND

EOARD Grant 13-3027

Report Date: September 2014

Final Report from 1 March 2013 to 28 February 2014

Air Force Research Laboratory
Air Force Office of Scientific Research
European Office of Aerospace Research and Development
Unit 4515, APO AE 09421-4515

REPORT DOCUMENTATION PAGE

Form Approved OMB No. 0704-0188

1. REPORT DATE *(DD-MM-YYYY)*	2. REPORT TYPE	3. DATES COVERED *(From – To)*
22 September 2014	Final Report	1 March 2013 – 28 February 2014

4. TITLE AND SUBTITLE

Quantifying Space Environment Interactions with Debris Objects using Observation Data Fusion Techniques

5a. CONTRACT NUMBER

FA8655-13-1-3027

5b. GRANT NUMBER

Grant 13-3027

5c. PROGRAM ELEMENT NUMBER

61102F

6. AUTHOR(S)

Thomas Schildknecht
Monika Hager

5d. PROJECT NUMBER

5d. TASK NUMBER

5e. WORK UNIT NUMBER

7. PERFORMING ORGANIZATION NAME(S) AND ADDRESS(ES)

UNIVERSITAET BERN
NON-PROFIT STATE UNIVERSITY
HOCHSCHULSTRASSE 4
BERN 3012 SWITZERLAND

8. PERFORMING ORGANIZATION REPORT NUMBER

N/A

9. SPONSORING/MONITORING AGENCY NAME(S) AND ADDRESS(ES)

EOARD
Unit 4515 BOX 14
APO AE 09421

10. SPONSOR/MONITOR'S ACRONYM(S)

AFRL/AFOSR/IOE (EOARD)

11. SPONSOR/MONITOR'S REPORT NUMBER(S)

AFRL-AFOSR-UK-TR-2014-0034

12. DISTRIBUTION/AVAILABILITY STATEMENT

Distribution A: Approved for public release; distribution is unlimited.

13. SUPPLEMENTARY NOTES

14. ABSTRACT

In this report, we describe the first steps towards the goal of quantifying space environment interactions with debris objects using observation data fusion techniques, namely the setup of an observation campaign to acquire lightcurves of geosynchronous artificial space objects. We first explain how the candidate objects were selected. Then we describe the acquisition of the observations, featuring technical details, the observation strategy and also the practical difficulties that we encountered along the way. Finally, we present the successfully acquired observations, giving a qualitative discussion of the obtained light curves and a quantitative discussion of the rotation periods for a number of sample objects. In order to quantify space environment interactions with debris objects using observation data fusion techniques, additional work is needed.

15. SUBJECT TERMS

EOARD, space observation, space debris, object characterization, astrodynamics, orbital evolution, HAMR objects, ZIMLAT telescope

16. SECURITY CLASSIFICATION OF:			17. LIMITATION OF ABSTRACT	18, NUMBER OF PAGES	19a. NAME OF RESPONSIBLE PERSON
a. REPORT	b. ABSTRACT	c. THIS PAGE			Kevin Bollino
UNCLAS	UNCLAS	UNCLAS	SAR	31	19b. TELEPHONE NUMBER *(Include area code)* +44 (0)1895 616163

Grant Number: FA8655-13-1-3027
Grant Period: 1 MARCH 2013 to 28 FEBRUARY 2014

Quantifying Space Environment Interactions with Debris Objects using Observation Data Fusion Techniques

Prof. Dr. Thomas Schildknecht / BSc Monika Hager
Astronomical Institute of the University of Bern

22 September 2014

Summary. In this report, we describe the first steps towards the goal of quantifying space environment interactions with debris objects using observation data fusion techniques, namely the setup of an observation campaign to acquire lightcurves of geosynchronous artificial space objects. We first explain how the candidate objects were selected. Then we describe the acquisition of the observations, featuring technical details, the observation strategy and also the practical difficulties that we encountered along the way. Finally, we present the successfully acquired observations, giving a qualitative discussion of the obtained light curves and a quantitative discussion of the rotation periods for a number of sample objects. In order to quantify space environment interactions with debris objects using observation data fusion techniques, additional work is needed.

List of Abbreviations

AIUB	Astronomical Institute of the University of Bern
AMR	Area-to-mass ratio
COSPAR	Committee on Space Research
GEO	Geosynchronous
HAMR	High area-to-mass ratio
TLE	Two-line elements
ZIMLAT	Zimmerwald Laser and Astrometry Telescope

Contents

List of Figures

List of Tables

1 Introduction

The broader context of this work is a project to eventually identify the sources and sinks of the population of high area-to-mass ratio (AMR) debris objects in high altitude orbits. Position data and optical light curves shall be fused and used to estimate the orbits, AMR, and attitude states of space objects in a common process.

The identification of the sources and sinks of the population of high AMR objects in high altitude orbits requires building up and maintaining an orbit catalogue of these objects. Current approaches use only position measurements to associate observations with objects in the catalogue and to determine their orbits including the critical AMR. The AMR of many of these objects is varying considerably in a currently unpredictable way probably as a result of changing attitude states. As a consequence many high AMR objects are lost. The project aims at improved orbit determination and prediction procedures by fusing position data and optical photometry data including light curves. In particular the project shall

- Explore possibilities to estimate the orbits, AMR, and attitude states of space objects in a common process by fusing position data and light curve observations. Novel orbit and attitude state determination algorithms shall be developed.

- Assess the benefits of this approach with respect to the classical approach of independently estimating these properties.

- Assess benefits of using estimated AMR and object albedo for the association of tracks and the correlation with the catalogue.

- Validate the developed algorithms and procedures with actual position and light curve measurements from the ZIMLAT telescope.

The work performed in the context of this grant consisted in the acquisition and classification of light curve measurements for a basic set of objects including active spacecraft and debris objects. This data set shall later serve as test bed to develop and explore the benefits of data fusion algorithms.

We first explain how the candidate objects were selected. Then we describe the acquisition of the observations. Finally, we present the results, giving a qualitative discussion of the obtained light curves and a quantitative discussion of the rotation periods for a number of sample objects.

We thank Dr. Jiri Silha and BSc Esther Linder for their contribution to Section 4.3 of this report.

2 | Selection of Candidate Objects

Candidate objects were selected from different groups. Operational, stable satellites as well as satellites out of service were chosen. Besides satellites of cylindrical shape, more complex, box-wing type satellites were included (see Figure 2.1). The selection also comprises upper stages of various, roughly cylindrical types (see Figure 2.2). Finally, some of AUIBs internal, so-called HAMR-objects[1] were included in the observation campaign.

The AIUB archive of lightcurves was searched for lightcurves with interesting features: Peaks of extreme brightness (these might result from highly reflecting components), signs of undersampling, lightcurves that vary over time, lightcurves showing periodicity and lightcurves showing a large variation in magnitude. Interesting objects with a long observation record were included accordingly. In addition, the object Z08343R, an object drifting along the GEO ring, was included.

We were not able to observe all of the selected objects. For some objects, two-line elements (TLE) were no more available, and some objects were not visible during the observation period. Furthermore, some of AUIBs internal HAMR-objects had not been observed for a certain period and could therefore not be found anymore.

Table 2.1 summarizes the objects that were successfully observed during the observation period (November 2013 to June 2014). The Cospar number, the number of observations, the shape and the status of the objects as well as the signature of the lightcurve is given. For the terms used to describe the lightcurves (last column of table 2.1), refer to Section 4.1.

[1] The area-to-mass ratio (AMR) is an important dynamical parameter. An object with an AMR value larger than 1 m^2/kg is considered a high area-to-mass (HAMR) object. Multilayer insulation foils of spacecraft are examples of HAMR-objects.

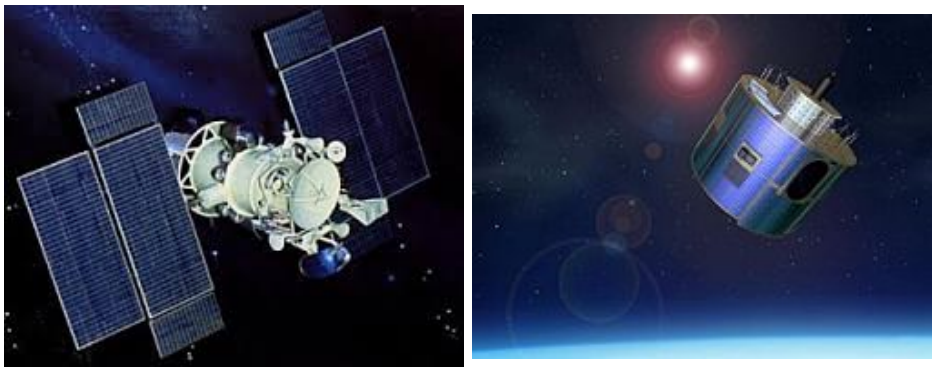

Figure 2.1: Box-wing type Gorizont (left) and cylindrical type Meteosat (right) satellite.

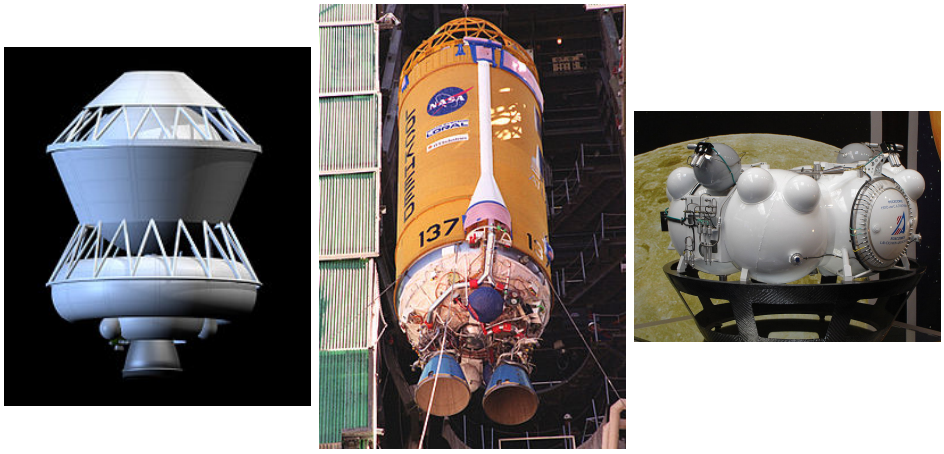

Figure 2.2: Upper stages: Blok DM-2 (left), Centaur (middle), Fregat (right).

	Cospar nb.	Name / AMR	nb. obs.	Shape	Status	Signature of lightcurve
1	02040B	Meteosat 8	3	cyl	op	$\Delta = 0.6m$
2	05049B	Meteosat 9	3	cyl	op	peaks, $\Delta = 0.6m$
3	00081A	Astra 2D	3	bw	op	$\Delta = 2.0m$, varying
4	94070A	Astra 1D	3	bw	op	peaks, $\Delta = 1.0m$
5	01029A	Artemis	3	bw	nop	$\Delta = 0.6m$
6	77108A	Meteosat 1	3	cyl	nop	$\Delta = 0.9m$
7	68116A	Intelsat 3	3	bw	nop	$\Delta = 3.9m$
8	73058A	Intelsat 4	2	bw	nop	$\Delta = 6.0m$, peaks, us
9	89052A	Gorizont 18	1	bw	nop	per, $\Delta = 7.0m$, peaks
10	90102A	Gorizont 22	3	bw	nop	per, $\Delta = 7.0m$, peaks, varying, us
11	80081A	Raduga 7	1	bw	nop	$\Delta = 1.0m$
12	92088A	Cosmos 2224	3	bw	nop	per, $\Delta = 3.5m$, varying
13	83059B	Nahuel I2	1	cyl	nop	$\Delta = 0.4m$
14	77108D	Meteosat 1	2	$\sim$ cyl		$\Delta = 0.6m$
15	88034D	Blok DM-2	1	$\sim$ cyl		$\Delta = 0.5m$, us
16	91010F	Blok DM-2	3	$\sim$ cyl		per, $\Delta = 1.0m$, us
17	99047E	Blok DM-2	1	$\sim$ cyl		per, $\Delta = 1.8m$, peaks, us
18	90061D	Blok DM-2	3	$\sim$ cyl		per, $\Delta = 0.7m$, us
19	08006C	Breeze-M R/B	1	$\sim$ cyl		$\Delta = 0.6m$
20	10002B	Breeze-M R/B	3	$\sim$ cyl		$\Delta = 0.5m$
21	10006B	Breeze-M R/B	2	$\sim$ cyl		$\Delta = 0.3m$
22	11001B	Fregat R/B	2	$\sim$ cyl		per, $\Delta = 3.5m$
23	11048B	Breeze-M R/B	2	$\sim$ cyl		$\Delta = 0.3m$
24	68050J	Titan 3C R/B	2	$\sim$ cyl		per, $\Delta = 3.6m$
25	68081E	Titan 3C R/B	1	$\sim$ cyl		per, $\Delta = 0.8m$, us
26	04015D	Blok DM-2	1	$\sim$ cyl		$\Delta = 0.8m$, us
27	09017B	Atlas 5 R/B	2	$\sim$ cyl		$\Delta = 4.0m$, us
28	12012D	Blok DM-2	3	$\sim$ cyl		$\Delta = 1.4m$, us
29	E06321D	2.5	1	?		per, $\Delta = 1.4m$, varying, us
30	E10040A	1.6	1	?		per, $\Delta = 1.0m$, varying
31	Z13222F	1.3	1	?		$\Delta = 0.8m$
32	Z08343R	0.008	3	?		per, $\Delta = 2.5m$, varying, us

Table 2.1: Successfully observed objects: stable satellites (1-4), instable satellites (5-13), upper stages (14-28), HAMR-objects (29-31), others (32); operational (op) or non-operational (nop) satellites, of cylindrical (cyl) or box-wing (bw) shape; upper stages of roughly cylindrical ($\sim$ cyl) shape.

3 | Observations

3.1 General Framework

Optical observations are performed at night when the wheather conditions are suitable. The observations are performed mainly by student observers which habe been specially trained for this task.

3.2 Instruments used

Observations of artificial space objects are performed with the 1 m Laser and Astrometry Telescope ZIMLAT, see Figure 3.1. The telescope is equipped with the CCD camera SI1100 with low readout-noise and high quantum efficiency. The limiting magnitude of the optical system is 19mag. More technical details can be found in [1].

3.3 Acquisition of Lightcurves

Lightcurves are obtained by taking series of small subframes (100x100 pixels or 1.29') centred on the objects. The exposure time for GEO-objects is around 1.5s, resulting in a sampling rate of around 3s. As the objects are of moderate brightness, no filters are used. On these subframes, the intensity of the object is measured. After 30 subframe images, an image with 2064x2048 pixels or 26.6' is acquired for calibration purposes. Furthermore, some time is needed for the readout of the data and the readjustment of the telescope (e.g. focus), resulting in a gap of around 20s between every two series of 30 subframes.

The observation data is stored in form of the original images, a textfile and a lightcurve. The original subframe image undergoes an automatic processing resulting in the exclusion of some images, e.g. if a star is present in the subframe or if the object is over- or underexposed. The textfile and the lightcurve are generated from the observation data of the remaining subframes. For the lightcurves featured in this report, no calibration

Figure 3.1: The ZIMLAT telescope at the Zimmerwald observatory.

has been applied. The resulting magnitudes are therefore to be understood as relative magnitudes, showing the magnitude variation.

3.4 Observation strategy

In order to learn something about the reproducibility of the observations, or, in other words, about the variability of the lightcurves, we planned to organize the frequency of the observations as follows. The objects should be observed multiple times in one night, once in consecutive nights or regularly over longer time periods.

In practice, this proved to be infeasible. The observation capacities were limited due to several reasons. With the ZIMLAT-telescope, three types of measurements are performed: besides the acquisition of lightcurves, it is also used for follow-up observations of space debris objects and for satellite laser ranging. This restricted the observation time available. The observation system had to be optimized and refined for our purposes. Serious software deficiencies and unforeseen hardware maintenance led to delays throughout the observation period. Last but not least, the wheather conditions this year have not been favorable for optical observations. Long periods of clear nights were the exception.

Nonetheless, 32 objects were observed in the observation period from November 2013 until June 2014. A maximum of three observations lasting 20 minutes each was performed for every object.

4 | Results

4.1 Qualitative Discussion of the Lightcurves

The newly acquired lightcurves have been analyzed visually, and the following features have been searched for:

periodic (per): The lightcurve shows a repeated brightness pattern.

Δm: The brightness fluctuation over an entire observation, read off the ordinate. Taken from the observation with the largest fluctuation, including possible peak values.

with peaks (peaks): The lightcurve shows measurement values of brightness significantly above (or below) average.

varying: The shape of the lightcurve varies significantly over time (i.e. for different observations).

undersampled (us): The lightcurve shows signs of undersampling (e.g. beats).

The result of this analysis is given in the last column of Table 2.1.

4.2 Detailed Analysis of Sample Lightcurves

Lightcurves of Meteosat 9 (05049B)

The Meteosat 9 satellite with Cospar number 05049B is cylindrically shaped, operational and stable. Three lightcurves of the object are displayed in Figure 4.1. The observation dates, phase angles and exposure times are given in Table 4.1. The lightcurves are flat, with fluctuations of around 0.1m and occasional peaks up to 0.3m. The peaks might stem from antenna structures on top of the satellite. The average magnitude seems to rise and decrase as a function of the phase angle.

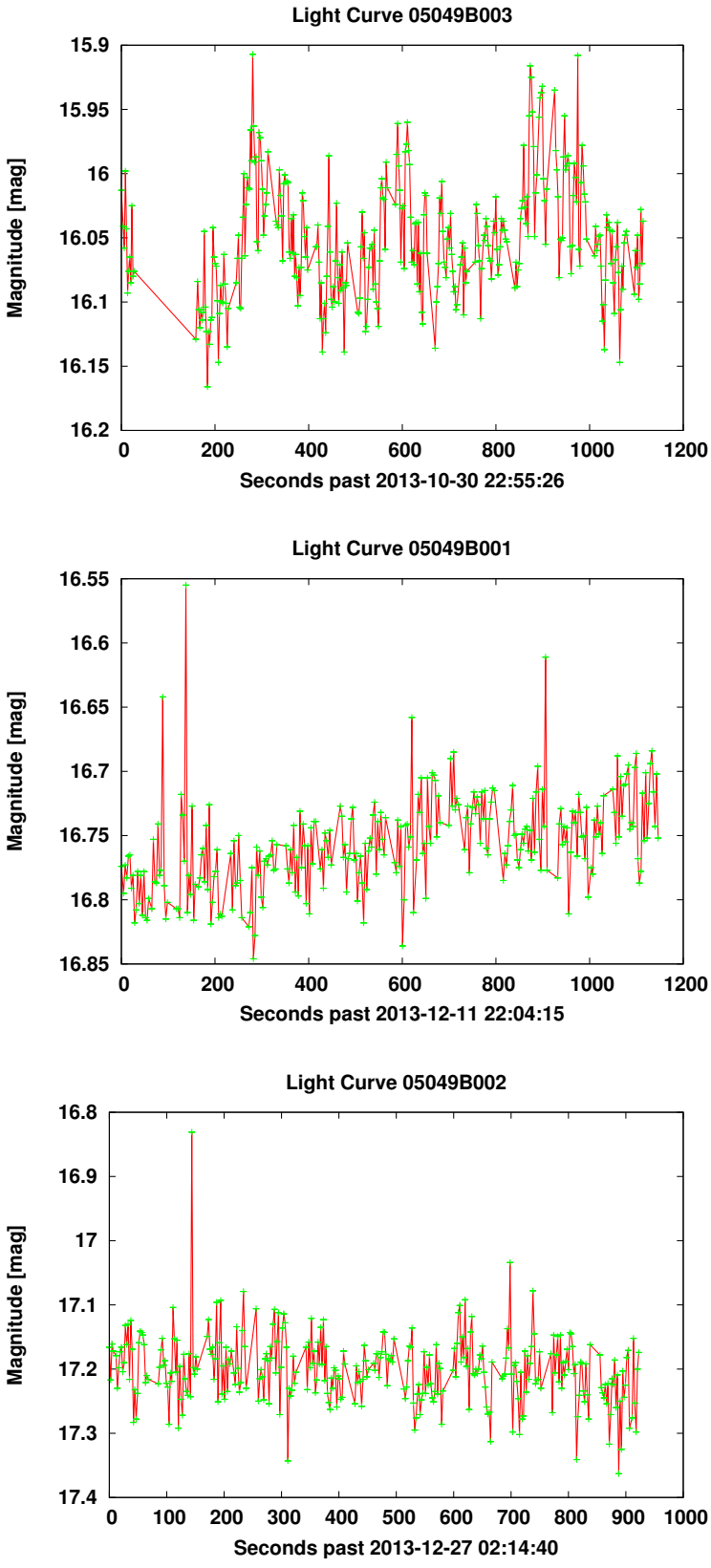

Figure 4.1: Lightcurves of Meteosat 9 (05049B).

Date	start epoch (MJD)	ϕ(deg)	exp.time / filter
Oct 30 2013	56595.96	21.0 to 20.8 to 20.9	1.5s / none
Dec 11 2013	56637.92	34.5 to 32.4	2.5s / none
Dec 26 2013	56653.10	51.6 to 54.7	1.5s / none

Table 4.1: Light curve measurements for object Meteosat 9 (05049B).

Date	start epoch (MJD)	ϕ(deg)	exp.time / filter
Dec 02 2013	56628.99.0	61.6 to 65.7	1.5s / none
Dec 10 2013	56636.98	54.1 to 58.1	1.5s / none
Apr 09 2014	56757.01	5.1 to 4.8 to 5.6	1.5s / none

Table 4.2: Light curve measurements for object Astra 1D 94070A.

Lightcurves of Astra 1D (94070A)

As the prevoiusly discussed object, the Astra 1D satellite (94070A) is operational and 3-axis stabilized. It is of box-wing shape. Three lightcurves of the object are displayed in Figure 4.2, and observation data is given in Table 4.2. The first observation shows larger magnitude fluctuations than the third one, which is essentially flat with single peaks of around 0.1m being the exception. In the first two lightcurves, a phase angle dependence of the average magnitude is visible.

Lightcurves of HAMR-object E10040A

For the HAMR-object E10040A, two lightcurves from the archive are compared to a recent one (see Table 4.3 and Figures 4.3. The lightcurve that was acquired in 2012 shows a period of around 70s and a magnitude variation of up to 3m. In the observation stemming from 2013, the magnitude varies only by 0.6m. The most recent lightcurve shows magnitude fluctuations around 0.3m and no periodicity. The lightcurve of this object seems to vary strongly over the years.

Lightcurves of upper stage 77108D

Archived observations of the upper stage 77108D show prominent magnitude peaks, while these are missing in the recently acquired observations (see Table 4.4 and Figures

Date	start epoch (MJD)	ϕ(deg)	exp.time / filter
Jul 18 2012	56126.89	84.1 to 79.6	5.0s / none
Jan 28 2013	56320.76	86.6 to 82.0	5.0s / none
Apr 01 2014	56748.91	3.5 to 7.0	3.0s / none

Table 4.3: Light curve measurements for HAMR-object E10040A.

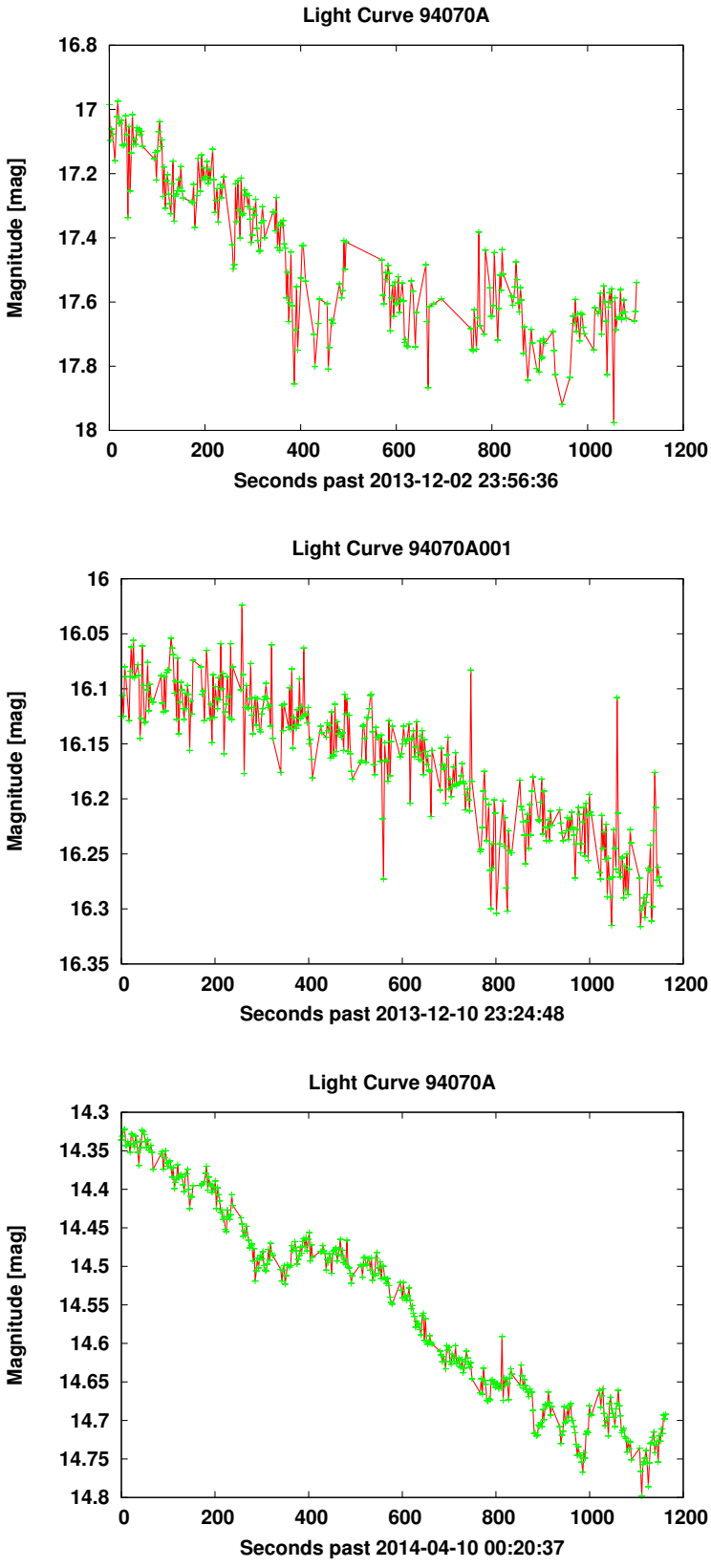

Figure 4.2: Lightcurves of Astra 1D (94070A)

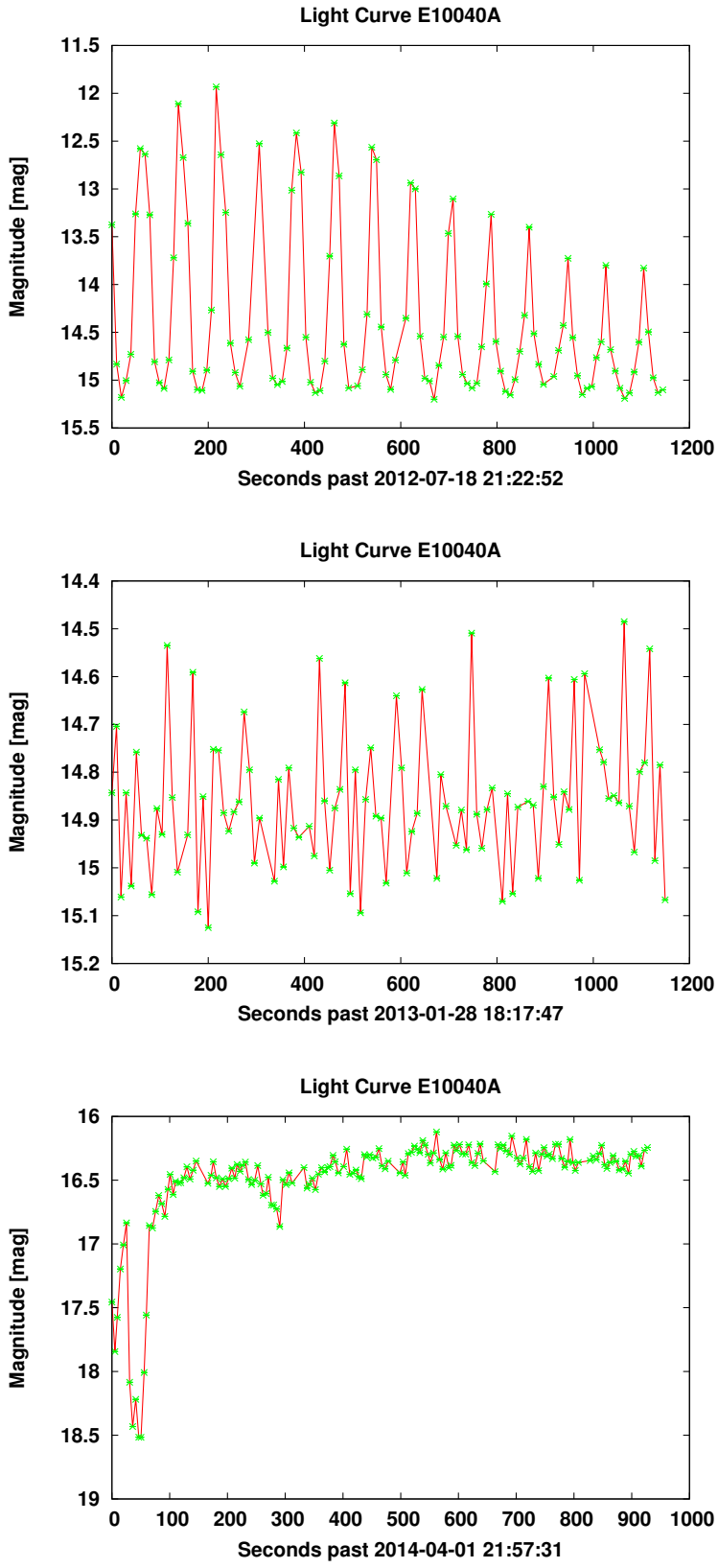

Figure 4.3: Lightcurves of HAMR-object E10040A

Date	start epoch (MJD)	ϕ(deg)	exp.time / filter
Feb 24 2008	54520.84	32.4 to 23.8	1.1s / none
Dec 07 2013	56633.04	19.4 to 15.6	1.5s / none

Table 4.4: Light curve measurements for upper stage 77108D.

Object	Date	start epoch (MJD)	ϕ(deg)	exp.time / filter
02040B	Oct 30 2013	56595.90	30.7 to 27.7	1.5s / none
68081E	Mar 14 2014	56731.05	15.8 to 17.2	1.5s / none
91010F	Nov 27 2013	56623.97	59.0 to 63.6	2.5s / none
E06321D	Apr 17 2014	56764.90	23.8 to 19.1	3.0s / none
Z08343R	Apr 17 2014	56764.87	42.4 to 37.8	3.0s / none

Table 4.5: Measurement data.

4.4).

4.3 Rotation Rates of Sample Objects

Sample observations have been analyzed with respect to rotation rates. Three techniques were used: Fourier transformation [2], the Welch method [3], [4] and the Periodogram [5], [6]. The five strongest periods were determined with each method. Matching periods[1] were submitted to further analysis. Some measurement data is given in Table 4.5, and the results of the analysis are summarized in Table 4.6. The lightcurves are shown in Figures 4.5 to 4.9.

Matching periods were ordered by their power in the Fourier spectrum. For the object 02040B, the observation gap (as explained in Section 3.3) caused a period around 80s, emanating from all three methods and visible by eye as well. Periods around 42 and 28 seconds resulted from calculations. These two periods might be artefacts, as they appear identically for the majority of the objects. In summary, the extraction of rotation rates seems to be difficult for a stable object like 02040B, whose lightcurve shows little structure.

For the object 68081E, the methods again found the observation gap, resulting in a period of around 80 seconds. Also the 42s- and 28s- periods were detected. The period of 16s can be confirmed by the eye and is a candidate for a physical rotation period.

Ignoring the observation gap and possible artefacts, we find a period of just under 70s for object 91010F, periods of around 40s and 10s for object E06321D, and periods around 70s and 30s for object Z08343R. All these periods are also visible to the eye.

[1] Periods of the Welch and Periodogram method with a ratio of 0.7 to 1.3 compared to the Fourier method were accepted.

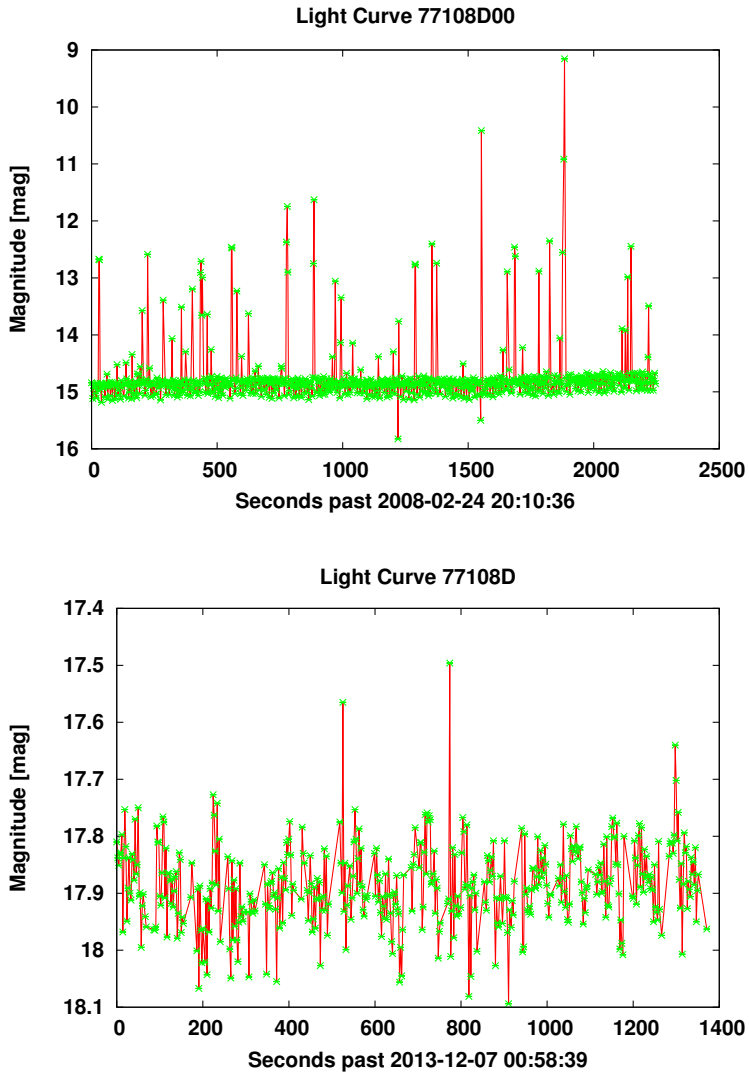

Figure 4.4: Lightcurves of upper stage 77108D.

Object	Fourier	Periodogram	Welch	By eye
02040B	84.9, 42.5, 28.3	87.2, 43.1	85.3, 42.7, 28.4, 21.3	80, 5
68081E	72.6, 40.8, 8.1, 27.2, 15.9	85.3, 42.7 8.1, 28.4	42.7, 8.3, 28.5, 16.0	80, 100, 15
91010F	103.6, 54.2, 67.0, 38.0, 28.5	120.5, 58.5, 38.6	64.0, 36.6, 28.4, 23.3	100, 70, 5
E06321D	63.2, 42.1, 113.8, 10.4	66.1, 44.5, 136.5, 10.6	64.0, 42.7, 10.7	140, 40, 10
Z08343R	66.8, 34.4, 113.5, 42.0, 23.2	73.1, 35.3, 136.5, 44.5	64.0, 36.6, 23.3, 18.3	120, 70, 30

Table 4.6: Periods in seconds calculated using Fourier Transformation, the Periodogram and the Welch method as well as seen by eye.

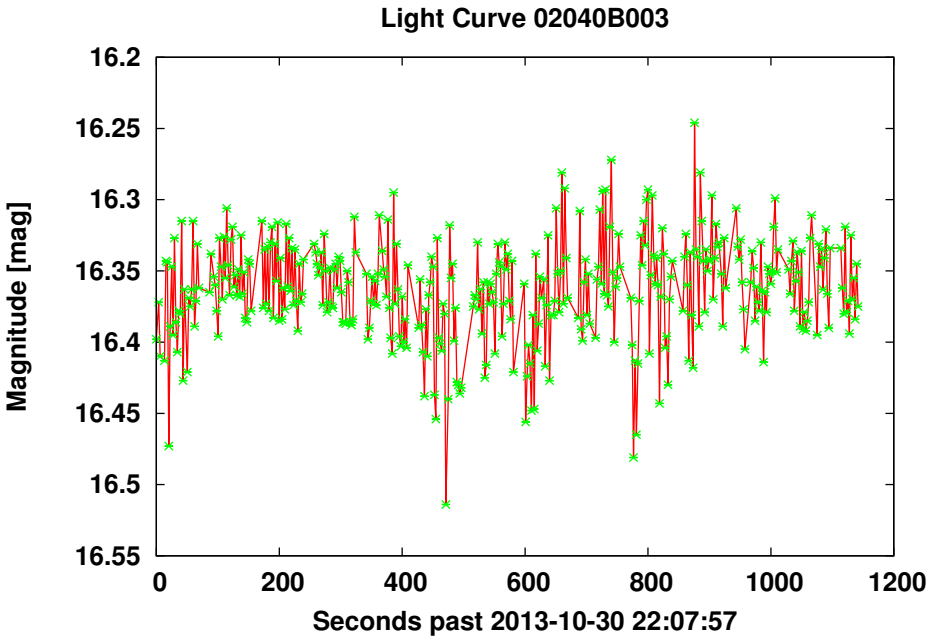

Figure 4.5: Lightcurve of Meteosat 8 (02040B).

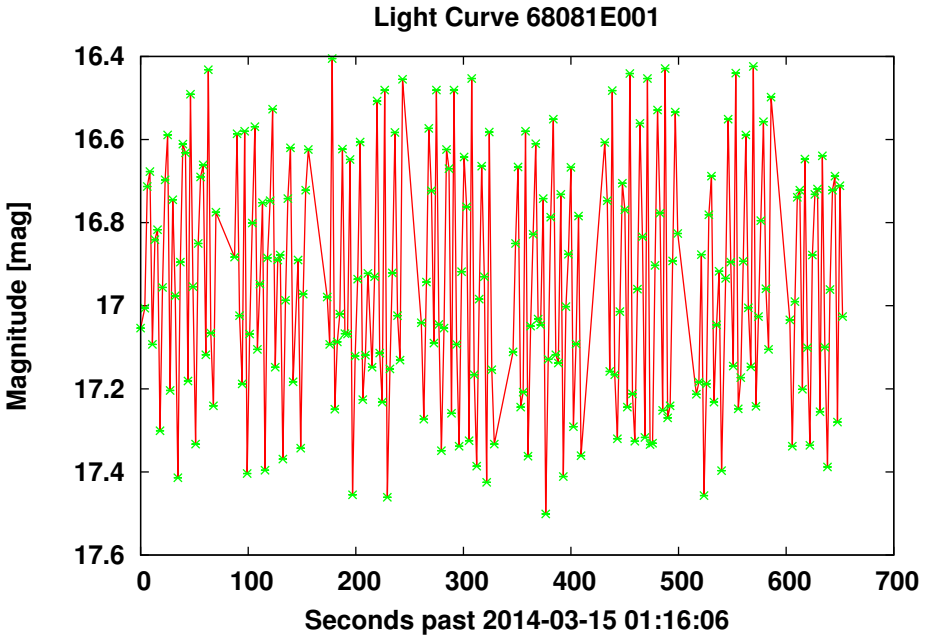

Figure 4.6: Lightcurve of Titan 3C (68081E).

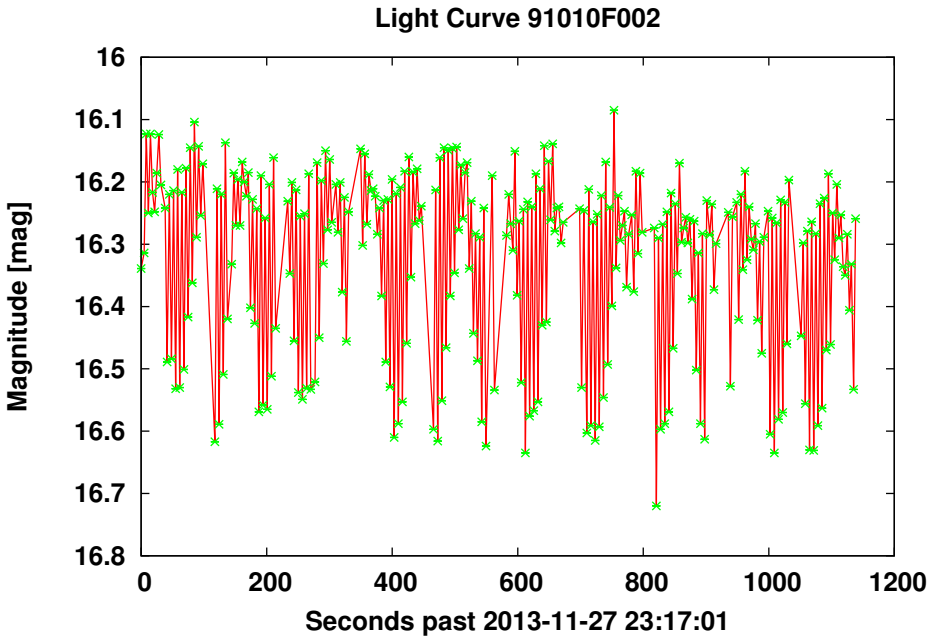

Figure 4.7: Lightcurve of Blok DM-2 (91010F).

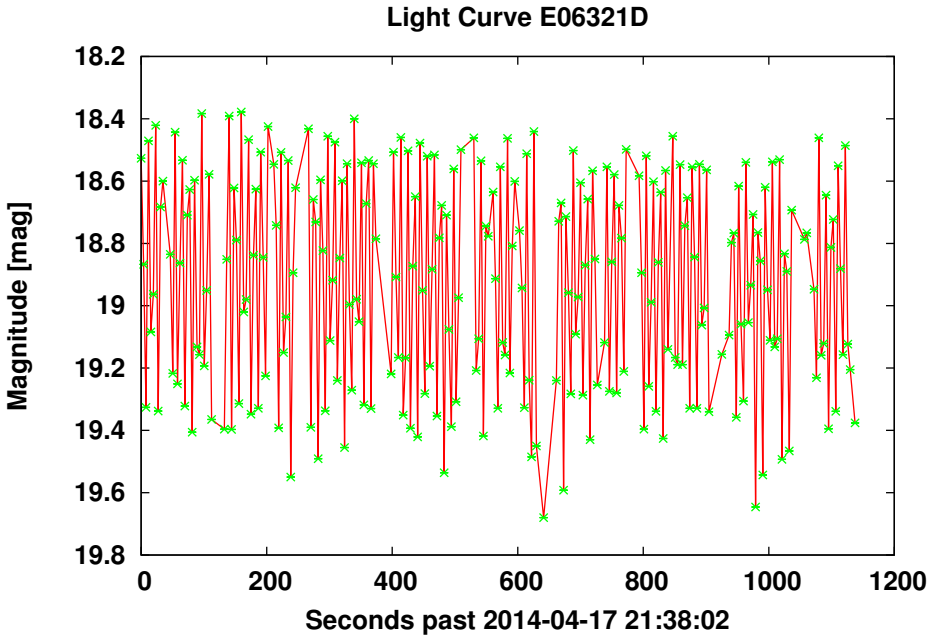

Figure 4.8: Lightcurve of HAMR-object E06321D.

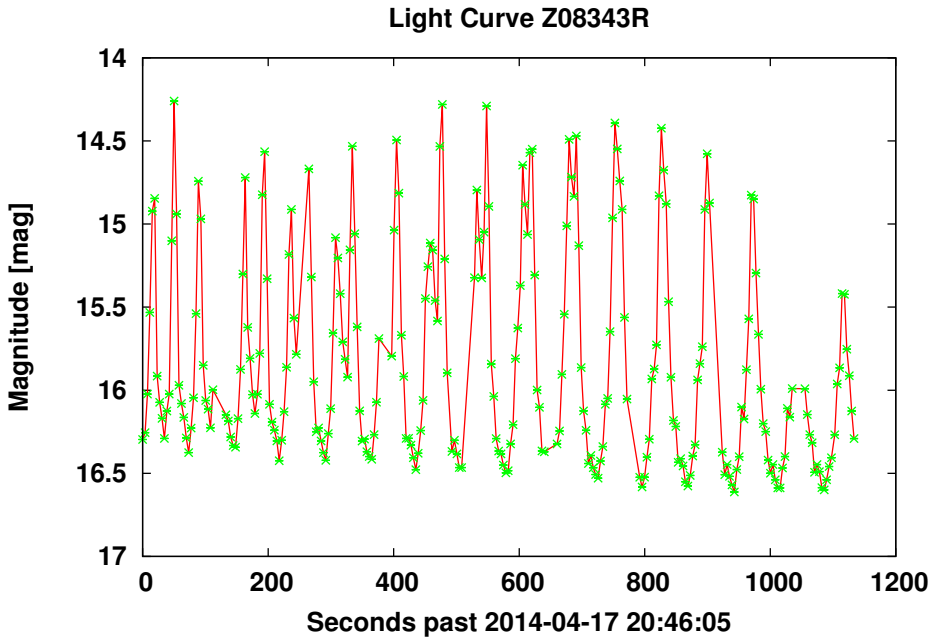

Figure 4.9: Lightcurve of object Z08343R.

5 | Conclusion

An observation campaign for GEO-objects has been set up, comprising a variety of space debris objects. The objects have been observed, despite the practical difficulties that arose during the observation period. From the observation data, lightcurves have been acquired and discussed qualitatively and quantiatively. While these are important steps towards a fusion of position data and light curve observations, a lot of work remains to be done.

Bibliography

[1] J. Herzog, T. Schildknecht, A. Hinze, M. Ploner, A. Vananti, *Space Surveillance Observations at the AIUB Zimmerwald Observatory.* Astronomical Institute, University of Bern.

[2] http://www.mathworks.ch/ch/help/matlab/ref/fft.html

[3] P. D. Welch, *The Use of Fast Fourier Transform for the Estimation of Power Spectra: A Method Based on Time Averaging Over Short, Modified Periodograms.* IEEE TRANSACTIONS ON AUDIO AND ELECTROACOUSTICS, VOL. AU-15, NO.2, JUNE 1967.

[4] http://www.mathworks.ch/ch/help/signal/ref/pwelch.html

[5] J. D. Scargle, *Studies in Astronomical Time Series Analysis. II. Statistical Aspects of Spectral Analysis of Unevenly Spaced Data.* The Astrophysica Journal, 263 : $835_8 53$, 1992 December 15.

[6] http://www.mathworks.ch/ch/help/signal/ref/periodogram.html